

SCIENTIFIC REPORTS

OPEN

Au Nanocage Functionalized with Ultra-small Fe_3O_4 Nanoparticles for Targeting T_1 – T_2 Dual MRI and CT Imaging of Tumor

Received: 10 March 2016

Accepted: 26 May 2016

Published: 17 June 2016

Guannan Wang^{1,2}, Wei Gao¹, Xuanjun Zhang² & Xifan Mei¹

Diagnostic approaches based on multimodal imaging of clinical noninvasive imaging (eg. MRI/CT scanner) are highly developed in recent years for accurate selection of the therapeutic regimens in critical diseases. Therefore, it is highly demanded in the development of appropriate all-in-one multimodal contrast agents (MCAs) for the MRI/CT multimodal imaging. Here a novel ideal MCAs (F-AuNC@ Fe_3O_4) were engineered by assemble Au nanocages (Au NC) and ultra-small iron oxide nanoparticles (Fe_3O_4) for simultaneous T_1 – T_2 dual MRI and CT contrast imaging. In this system, the Au nanocages offer facile thiol modification and strong X-ray attenuation property for CT imaging. The ultra-small Fe_3O_4 nanoparticles, as excellent contrast agent, is able to provide great enhanced signal of T_1 - and T_2 -weighted MRI ($r_1 = 6.263 \text{ mM}^{-1} \text{ s}^{-1}$, $r_2 = 28.117 \text{ mM}^{-1} \text{ s}^{-1}$) due to their ultra-refined size. After functionalization, the present MCAs nanoparticles exhibited small average size, low aggregation and excellent biocompatible. *In vitro* and *In vivo* studies revealed that the MCAs show long-term circulation time, renal clearance properties and outstanding capability of selective accumulation in tumor tissues for simultaneous CT imaging and T_1 - and T_2 -weighted MRI. Taken together, these results show that as-prepared MCAs are excellent candidates as MRI/CT multimodal imaging contrast agents.

The development of personalized therapeutical approaches and the increasing precision of surgical techniques indicate the importance of multimodal imaging to assist physicians in diagnosis and monitoring the response to therapy. In particular, noninvasive imaging (eg. MRI and CT) and minimally invasive *in vivo* bioimaging techniques are valuable tools in the arsenal of clinical diagnostics^{1–3}. The new emergence of MRI/CT scanner (eg. General Electric CT & MRI scanners) allows doctors to get more precise information of tumor localization and boundary identification by combination of MRI and CT imaging. Accompanied with the development of imaging technology, high-performance, especially those all-in-one multimodal contrast agents (MCAs) are highly demanded for accurate diagnosis and therapy. In the past several years, various of MCAs based on Au and Fe_3O_4 nanoparticles have been developed for *in vivo* and pre-clinical MRI/CT imaging with the purpose of increasing the contrast of lesion, because these nanoparticles can offer facile thiol modification, enhanced chemical stability, excellent biocompatibility, superparamagnetic capability, and strong X-ray attenuation property^{4–12}. However, the achievement of these MCAs by using Fe_3O_4 and Au shell always have low MRI contrast capability, because common Fe_3O_4 can only provide T_2 weight MRI with dark imaging and Au shell coated on the surface of Fe_3O_4 also prevent the connection with water molecules in tissue resulting in the reduction of the MRI contrast signal.

To address above problem, here we have exploited a new folic acid functionalized MCAs (F-AuNC@ Fe_3O_4), based on Au nanocages (AuNCs) and ultrasmall Fe_3O_4 nanoparticles, to associate in one signal nanosystem several different properties, such as, tumor targeting, bright T_1 and dark T_2 dual MRI contrast enhancement, and X-ray attenuation (Fig. 1). Compared with other multimodal imaging systems, our presented MCAs are the first engineered for simultaneous T_1 – T_2 dual MRI and CT contrast. The simultaneous T_1 and T_2 weight contrast imaging could great enhance the sensitivity of MRI to give the comprehensive high spatial resolution of soft tissue information for tumor contour and localization, while the real-time and three-dimensional high spatial

¹College of Pharmacy & the Key Laboratory for Medical Tissue Engineering of Liaoning Province, Liaoning Medical University, Jinzhou, 121001, China. ²Faculty of Health Sciences, University of Macau, Avenida da Universidade, Taipa, Macau, China. Correspondence and requests for materials should be addressed to G.W. (email: chemwangguannan@gmail.com) or X.M. (email: meixifan1971@163.com)

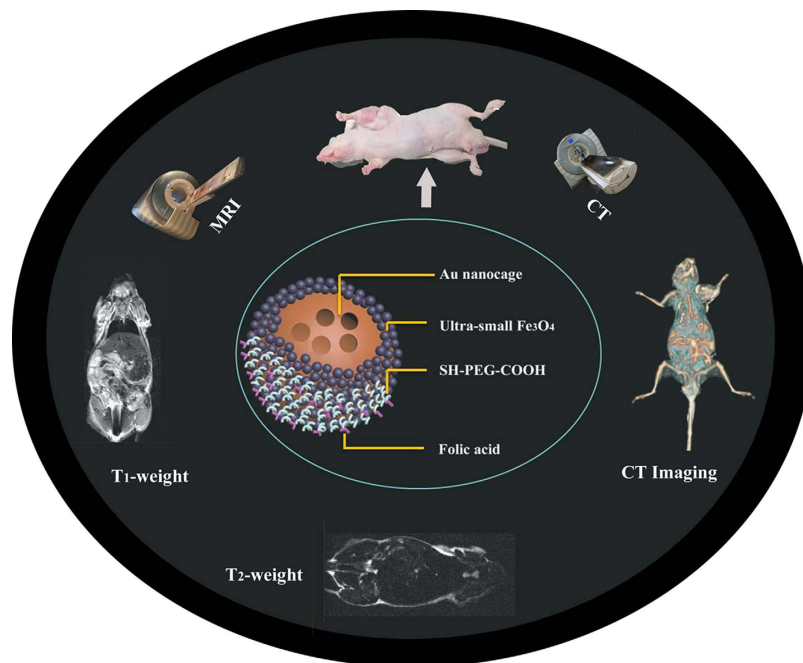


Figure 1. The illustration of MCAs (F-AuNC@Fe₃O₄) for targeting multimodal imaging of tumor.

resolution of hard tissue information for tumor contour and localization could be provided by CT imaging. The use of noninvasive imaging like MRI and CT, possible with our MCAs, can provide the complementary information necessary for accurate evaluation of the tumorigenesis areas, which is one of the major challenges of diagnostic imaging.

Results and Discussion

Synthesis and Characterization of F-AuNC@Fe₃O₄. It has been demonstrated that the size control and further surface functionalization are two key factors in the development of high-performance nanoprobe for tumor targeting¹³. Because AuNC@Fe₃O₄ has no selectivity toward tissues and is unable to discriminate between malignant and nonmalignant tumors, conjugation of specific bimolecular (folic acid) with AuNC@Fe₃O₄ has been employed to improve their lesion targeting selectivity. The final nanoparticles were purified by gel filtration using Sephacryl HR-300 gel medium.

High-resolution transmission electron microscopy (HRTEM) images of the ultra-small sized Fe₃O₄ nanoparticles and Au nanocage are shown in Figs S1 and S2 (Supporting Information). The average diameter of the Fe₃O₄ nanoparticles is around 2.2 nm with high uniformity, which could provide simultaneous T₁ and T₂ weight MRI contrast imaging proved in our previous work⁹. Au nanoparticles exhibit perfect nanocage structure with outer diameters of around 50 nm¹⁴. After assembled together, the HRTEM and SEM of final F-AuNC@Fe₃O₄ are shown in Fig. 2a,b,d, which clearly show that the prepared F-AuNC@Fe₃O₄ have hollow structure with rough morphology and they exhibit narrow distribution size around 70 nm. Compared with Au nanocages, it is obviously that the surface of F-AuNC@Fe₃O₄ was deposited with ultrasmall Fe₃O₄ nanoparticles. From the inset of Fig. 2b, the HRTEM of the edge of F-AuNC@Fe₃O₄, we can also clearly see that the small Fe₃O₄ nanoparticles around 2 nm are conjugated with Au nanocages. The energy-dispersive X-ray (EDX) spectrum of F-AuNC@Fe₃O₄ (Fig. 2c) also confirms the existence of elements O and Fe from Fe₃O₄, Au and Ag from the Au nanocages. The structure of F-AuNC@Fe₃O₄ can give enough space to let Fe₃O₄ nanoparticles connect with water molecular in tissue to produce high MRI signals due to the Fe₃O₄ nanoparticles assembled on the outer surface of Au nanocage; and at the other hand, the nanocages structure also gives their high surface to volume ratio, which also could benefit CT signal enhancement^{15,16}. The Dynamic light scattering (DLS) (Fig. 2e) showed that the hydrodynamic diameter of F-AuNC@Fe₃O₄ was around 110 nm, which indicated that they have smaller size in aqueous without any aggregation and could process reasonable blood circulation time and good lesion accumulation rate¹³. Inductively coupled plasma mass spectrometry (ICP-MS) study revealed that weight percentages of Au and Fe₃O₄ encapsulated were 58.2 and 17.2%, respectively.

The UV-vis absorption spectra of the Au nanocage and F-AuNC@Fe₃O₄ in aqueous suspension are shown in Fig. 2f, and the absorption spectra of ultra-small sized Fe₃O₄ nanoparticles is provided in Fig. S3 (Supporting Information). Here, Au nanocages and F-AuNC@Fe₃O₄ exhibits very strong and broad absorption from 600 nm to 800 nm with the maximum absorption at around 750 nm. After deposition of ultra-small sized Fe₃O₄ nanoparticles onto the surface of Au nanocage, a new broad absorption band appears in the spectrum of F-AuNC@Fe₃O₄, which is contributed by the strong absorption of Fe₃O₄ nanoparticles in visible spectral region¹⁷.

CT, Relaxometric and Biocompatible Properties. CT and MRI images of F-AuNC@Fe₃O₄ nanoparticles at various concentrations in PBS solution were studied. F-AuNC@Fe₃O₄ possesses intrinsic advantages for

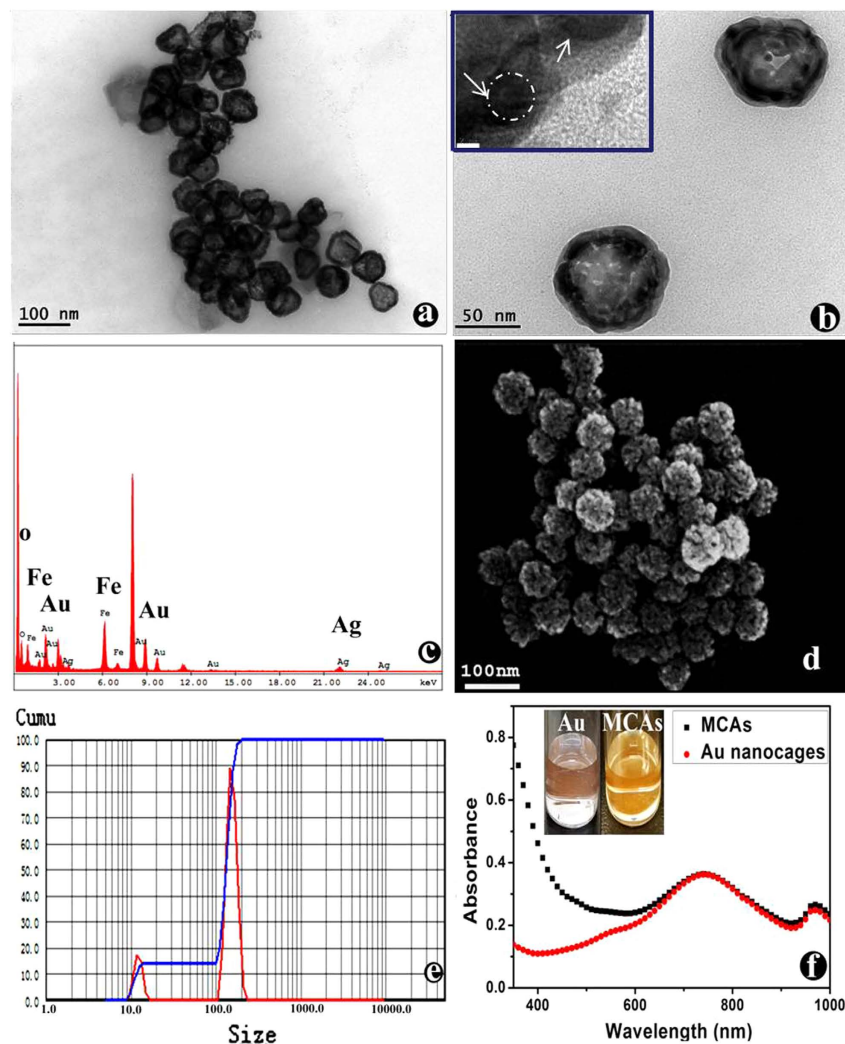


Figure 2. The characterizations of MCAs(F-AuNC@Fe₃O₄): TEM (a,b) (The inset is the High Resolution TEM); EDX (c); SEM (d); DLS (e) and UV-vis absorption of Au nanocages and MCAs (the inset is digital images under daylight).

X-ray CT imaging owing to the larger X-ray absorption efficiency of Au element. As known, the higher the atomic number and electron density is, the higher the attenuation coefficient is. Therefore, the developed F-AuNC@Fe₃O₄ was expected that have the good imaging ability in X-ray CT imaging. The X-ray attenuation (CT) potency of these F-AuNC@Fe₃O₄ with various concentrations of Au was examined and the pure Au nanoparticles (ca. 50 nm in diameter) were used as a control. It is clearly that the CT signal of F-AuNC@Fe₃O₄ increase in a concentration dependent manner (Fig. 3b,c). Interestingly, the F-AuNC@Fe₃O₄ exhibit higher X-ray attenuation potency than that of bare Au NPs at the same concentration. According to previous reports, smaller Au nanoparticles exhibited more pronounced X-ray attenuating capability than the larger one, which caused by the high surface to volume ratio and mainly contributed to X-ray attenuation^{4,16}. Therefore, the enhanced CT contrast of F-AuNC@Fe₃O₄ compared to Au solid nanoparticle is attributed to their hollow and cage structure.

Moreover, we next evaluated the contrast capability of as prepared F-AuNC@Fe₃O₄ for T_1 and T_2 weight MRI at different Fe concentrations. The relaxation efficiencies are calculated by measuring the longitudinal and transverse relaxation rates (r_1 and r_2) of the proton signals of the F-AuNC@Fe₃O₄. As shown in Fig. 3d,e, F-AuNC@Fe₃O₄ exhibits a high r_1 value of 6.263 and an r_2 value of 28.117 mM⁻¹ s⁻¹. The high r_1 relaxivity of F-AuNC@Fe₃O₄ all can be attributed to the large number 5 unpaired electrons of Fe³⁺ ions on the ultra-small Fe₃O₄ nanoparticle surface⁵. The r_2/r_1 ratio is also an important parameter to evaluate the efficiency of T_1 contrast agents. The r_2/r_1 ratio of F-AuNC@Fe₃O₄ was 4.48 demonstrating that it can be efficient T_1 contrast agents. Although there are other nanomaterials based on Fe₃O₄-Au for biomedical imaging⁴⁻⁷, as we know F-AuNC@Fe₃O₄ is the first example that exhibits high r_1 relaxivity value for T_1 -weight MR enhanced imaging. Figure 3a also demonstrated the T_1 and T_2 modal MR images of F-AuNC@Fe₃O₄ with different Fe ion concentrations. The signal enhancement progressively increases with increasing of the F-AuNC@Fe₃O₄ concentrations, which manifests the potential of F-AuNC@Fe₃O₄ as powerful multifunctional contrast agent for T_1 and T_2 MRI.

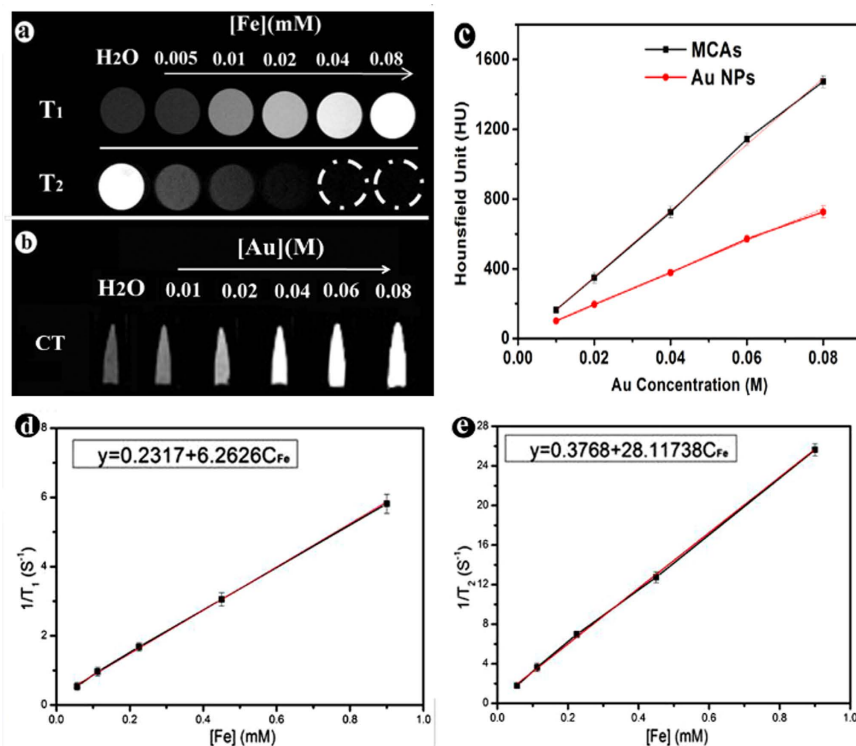


Figure 3. MRI and CT contrast ability of MCAs (F-AuNC@Fe₃O₄). (a) T₁ and T₂ weighted MR images of MCAs with different Fe ions concentrations. (b) CT imaging with different concentration of Au concentrations. (c) Plot of X-ray attenuation in Hounsfield units (HU) as a function of Au concentration of MCAs (black squares), compared to pure gold nanoparticles (red circles). (d,e) Plot of 1/T₁ and 1/T₂ over Fe concentration of as synthesized MCAs.

For biomedical applications, it is necessary to guarantee the hemocompatibility and cytocompatibility^{7,18}. Hemolytic assay and cell viability was used to assess the biocompatibility of the F-AuNC@Fe₃O₄, the results (Figs S4 and S5, Supporting Information) show synthesized F-AuNC@Fe₃O₄ have almost negligible damage to the red blood cells (<5% hemolytic activity) and have little toxicity to human lung cancer cell line A549 and normal human umbilical vein endothelial cells.

In vitro cellular uptake assay. The targeting ability of F-AuNC@Fe₃O₄ to folate receptor-overexpressed cancer cells was studied using A549 cells as an example. To more directly display the targeting capabilities of the F-AuNC@Fe₃O₄, the fluorescence Cy5-PEG-SH was selected to label the nanoparticles. In order to give clear fluorescence imaging and retain the ability of bio-functionalization, firstly, the mixture of COOH-PEG-SH and fluorescence Cy5-PEG-SH with 9:1 ratio was used to functionalize the surface of AuNC@Fe₃O₄, and then fluorescent AuNC@Fe₃O₄ was conjugated with targeting molecular folic acid to form the fluorescent F-AuNC@Fe₃O₄ for targeting cancer cell. As a control group, the fluorescent AuNC@Fe₃O₄ without surface folic acid also was used, which showed similar physical properties to those of fluorescent F-AuNC@Fe₃O₄. Figure 4a,b row show the confocal images of A549 cells after incubation with fluorescent F-AuNC@Fe₃O₄ and AuNC@Fe₃O₄ suspensions at a concentration of 0.5 mg/mL for one hour, respectively. The fluorescence image shown in Fig. 4a(i) clearly shows the successful internalization of the fluorescent F-AuNC@Fe₃O₄ into A549 cells. The much brighter red emission observed in Fig. 4a(i) as compared to that in Fig. 4b(i) (A549 cell incubation with fluorescent AuNC@Fe₃O₄) indicates that more F-AuNC@Fe₃O₄ can be internalized into A549 cells via folate receptor-mediated endocytosis, and the F-AuNC@Fe₃O₄ have more capability for cancer targeting recognition. These results confirm the F-AuNC@Fe₃O₄ can be effectively targeted to the folate receptor expressed cancer cells.

In vivo CT, T₁ and T₂ modal MR Imaging. For *in vivo* CT imaging, the CT imaging and CT value of the important organ regions were recorded before injection and at different time points post injection (Fig. 5a,b). Compared with the image of pre-injection, a great contrast enhancement was observed in the mouse body, tail vein and tumor region at 0.5 hour after injection, (Fig. 5a), demonstrating that the as synthesized F-AuNC@Fe₃O₄ can do enhance CT imaging in the circulating system. It is noted that the F-AuNC@Fe₃O₄ have a clear tendency of accumulation in the tumor tissue, the time-dependent distribution of the F-AuNC@Fe₃O₄ in the mouse was also tracked by CT signal value after intravenous injection. At timed intervals, the evident enhancement of the signals in different organs could be seen in Fig. 5b, the kidney and tumor imaging were greatly enhanced from 0.5 h to 6 h, and HU value of them rose from 95 to 464 and 213 to 730, respectively, while the signal value in other organs shows little fluctuation. A more careful look at the 3D-renderings of CT images, after post injection 6 h, the CT

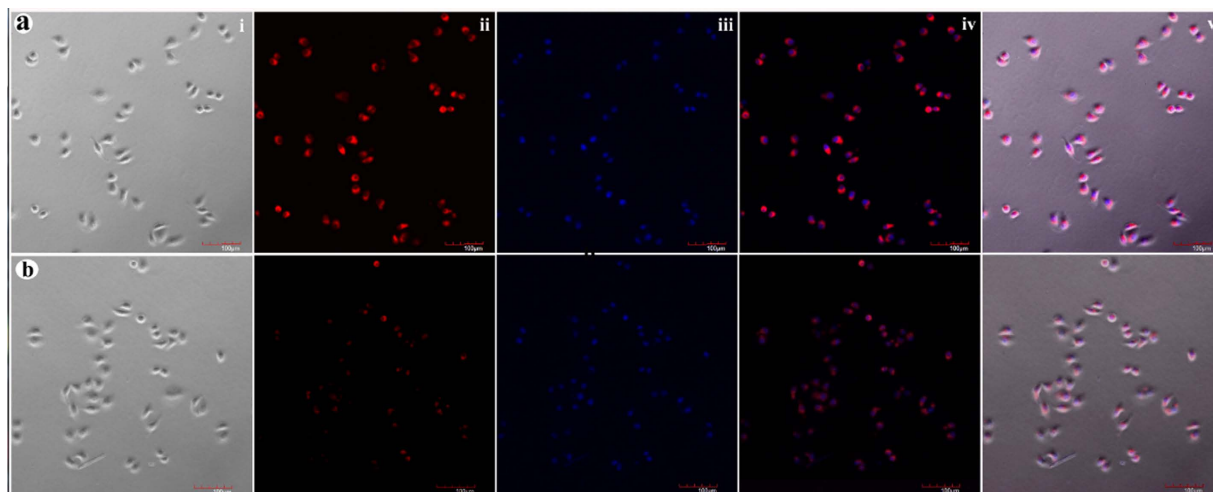


Figure 4. Confocal images of the A549 cells after one hour incubation with the 0.5 mg/mL of fluorescent F-AuNC@Fe₃O₄ (a); 0.5 mg/mL of fluorescent AuNC@Fe₃O₄ (b). The horizontal images were in this sequence: bright field (i), the red fluorescence field (ii), the nuclei stained by DAPI (iii), overlay of DAPI and fluorescence (iv), overlay of all (v). Scale bars are 100 μm.

contrast intensity in the body and organs of mouse obviously decrease over time, while the region of the tumor tissue is still labeled and CT imaging of bladder organ are suddenly clear, showing the excellent tumor targeting and renal clearance properties of F-AuNC@Fe₃O₄. The slow elimination of F-AuNC@Fe₃O₄ from blood during circulation is attributed to their optimal particle size and surface functionalization. The results demonstrate that the F-AuNC@Fe₃O₄ have the feasibility to be served as an *in vivo* CT contrast agent to provide the real-time and 3D-high spatial resolution imaging.

For tumor targeting T_1 and T_2 modal MR imaging, the F-AuNC@Fe₃O₄ with higher r_1 and r_2 relaxivity are expected to enhance the T_1 and T_2 modal MRI and to ease the toxicity with a decreased dose. T_1 and T_2 modal MRI of tumor-bearing mice were also recorded at various time intervals: before injection, 0.5, 1 and 6 hours after injection, as shown in Fig. 6a. Compared with pre-injection, we could observe a great contrast enhancement (brighten on the T_1 -weighted and darken on the T_2 weighted MR images) in the mouse body after post injection, demonstrating that as synthesized F-AuNC@Fe₃O₄ can simultaneously enhance T_1 and T_2 relaxation in the circulating system. The enhanced signal of blood vessel can be maintained for more than 6 h, which is much longer than that of Gd complex small molecules with a high excretion rate (about several minutes in small animals)^{9,19}. These results show that F-AuNC@Fe₃O₄ can also be used for long-term blood pool T_1 and T_2 modal MRI contrast agent, which is very important in clinical MR imaging^{20,21}. The long-term effect is also critical to obtain high-resolution and steady state images. Similar with the CT imaging, after 6 h, the T_1 and T_2 contrast intensity in the body of mouse obviously decrease over time, while the contrast intensity in the region of tumor increased over time, which confirm the F-AuNC@Fe₃O₄ have a tendency to be enriched in the tumor tissue.

In general, once injected intravenously, the contrast agents are easily accumulated in liver and spleen tissues²². Therefore, to provide further support of tumor targeting ability as well as information on the biodistribution of the F-AuNC@Fe₃O₄, both tumor and important organs such as heart, liver, spleen, kidney and tumor were harvested after the *in vivo* experiments, and the MRI with T_1 and T_2 modal was shown in Fig. 6b, respectively. At first, the much higher T_1 and T_2 signals in the tumor tissue compared to those from other organs further confirm the specific targeting of the FMNPs to the tumor. And then, the imaging signal of organs might be difference between MRI imaging and CT imaging, which is why we integrate MR imaging with CT imaging for achieving their complementary imaging features.

Histological study. An essential feature of MCAs is their biocompatibility, hence primary organs of tumor bearing mice post the administration of F-AuNC@Fe₃O₄ were tested via the pathological assay (H&E staining). In Fig. 7, the accumulation of F-AuNC@Fe₃O₄ was obviously observed in kidney, bladder and tumor (original magnification $\times 100$), but it was little even absence in liver and heart at 6 h post the injection, which is in consistent with our *in vivo* imaging findings. In addition, no observable morphological changes were seen in these organs, which ruled out the presence of acute injury induced by the injection of F-AuNC@Fe₃O₄.

In summary, water-dispersible F-AuNC@Fe₃O₄ nanoparticles-based multimodal contrast agent has been developed for synergistically multimodal imaging of tumor. To the best of our knowledge, this is the first time that ultra-small sized Fe₃O₄ and Au nanocages were assembled together to provide simultaneous CT imaging and T_1 and T_2 -modal MRI of tumor bearing mice. As a result, due to the small sizes and surface modification, the as-prepared F-AuNC@Fe₃O₄ preferentially accumulate in the tumor, and can be rapidly eliminated from the body via the renal system. The experimental results suggest the potential of F-AuNC@Fe₃O₄ as a safe and efficient contrast agent for biomedical applications such as multi-modality imaging and molecular diagnostics of diseases *in vitro* and *in vivo*, as well as theranostic applications.

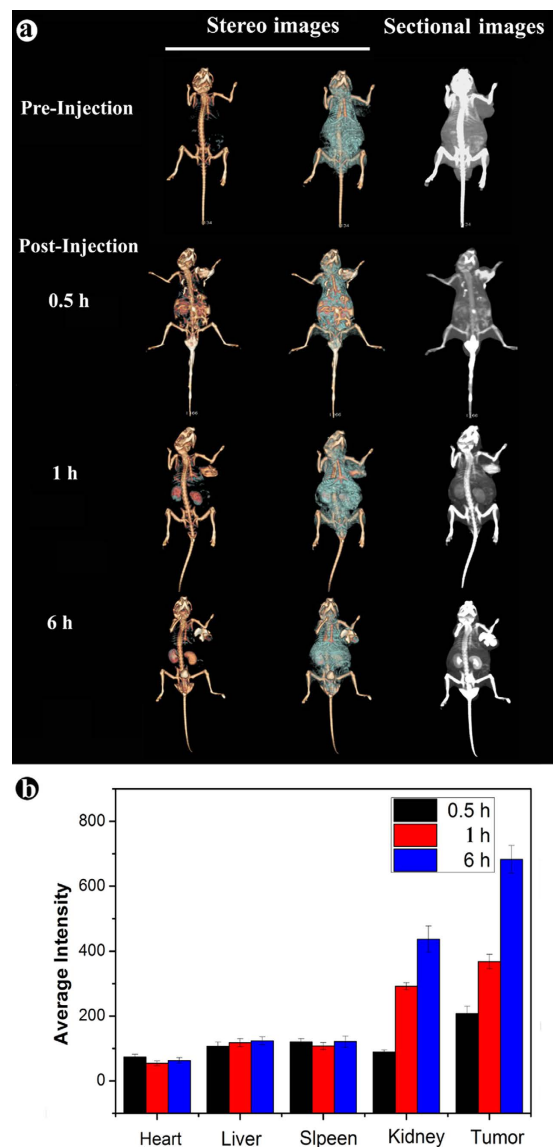


Figure 5. *In vivo* CT images of nude mice bearing tumor after intravenous injection of Au NPs at different timed intervals (pre-injection, 0.5 h, 1 h and 6 h post-injection), respectively (a) The HU average intensity of some organs (Heart, Liver, Spleen, Kidney, Tumor) after intravenous injection of Au NPs at different timed intervals.

Methods

All experimental protocol including any relevant details were approved by the Regional Ethics Committee, Liaoning Medical University, Liaoning Province, China.

Materials and Instrumentations. All of the chemicals and solvents were purchased from Sigma-Aldrich unless indicated otherwise. Transmission electron microscope (TEM) and energy dispersive X-ray (EDX) analyses were recorded using a FEI TECNAI G20 high-resolution transmission electron microscope operating at 200 kV. The samples were prepared by depositing a drop of a diluted colloidal solution on a carbon grid and allowing the liquid to dry in air at room temperature. Scanning electron microscope (SEM) data was collected by Hitachi Limited S4800. Dynamic light scattering (DLS) measurement was performed on a Malvern Zetasizer NANO ZS. UV-vis spectroscopy was carried out with SpectraMax[®] M5 Microplate Reader using 96-well plate. The relaxation measurements were performed on a Bruker minispec mq60 NMR analyzer at 40 °C using a magnetic field of 1.41 T. Samples were diluted in MilliQ water to different Fe and Au concentrations in the approximate range, and the absolute concentrations were determined afterwards by ICP-MS.

Synthesis of Gold Nanocages (AuNCs). Herein, Au cages with hollow structures using Ag nanocubes as sacrificial templates have been prepared according to previous methods¹². For all of the experiments, we used Au nanocages of mean 50 nm size together with a pore size of 2–3 nm. Briefly, 500 μ L of the Ag nanocubes (3 nM) was added to 5 mL of deionized water containing poly (vinyl pyrrolidone) (PVP, 1 mg mL⁻¹) hosted in a 50 mL flask

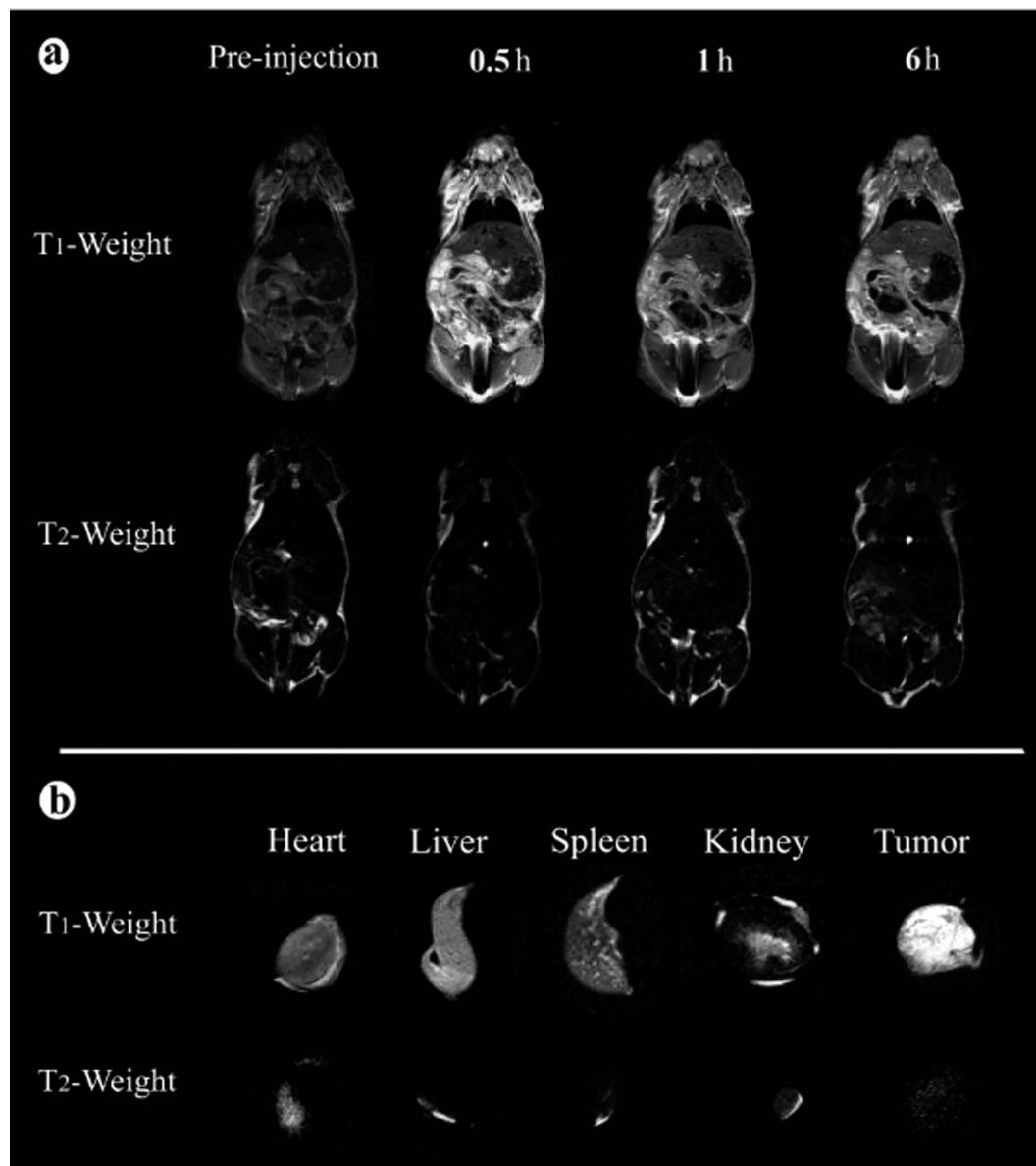


Figure 6. *In vivo* T_1 and T_2 weight MRI images of nude mice bearing tumor after intravenous injection of F-AuNC@Fe₃O₄ at different timed intervals (a); The T_1 and T_2 weighted MR images of various organs from the mice treated with F-AuNC@Fe₃O₄ after 6 h post-injection.

under magnetic stirring and then heated to boil for 10 min. Then around 4 mL of aqueous solution of HAuCl₄ (0.1 mM) was added to the flask at a rate of 0.75 mL min⁻¹ until the solution had an optical extinction peak at 755 nm as confirmed by UV spectroscopy. The solution was refluxed for another 10 min until the color of the reaction was stable. Once cooled to room temperature, the sample was centrifuged and washed with saturated NaCl solution to remove AgCl and with water several times to remove PVP and NaCl. For the further experiment, The PVP was replaced on nanocages with 2-aminoethanethiol to obtain AuNC-NH₂.

Synthesis of AuNC@Fe₃O₄. In a typical experiment for the synthesis of 2.2 nm sized ultra-small Fe₃O₄ particles was prepared according to our previous experiment. First, the polymer poly(acrylic acid) (PAA, 5.56 mmol) was dissolved in Milli-Q water (50 mL) in a 100 mL three-necked flask bubbled with nitrogen air for 40 min to remove oxygen. Then the solution was heated up to 80 °C. Meanwhile, Ferric salt (0.54 mmol) and Ferrous salt (0.279 mmol) as iron precursors was quickly injected into the hot polymer solution under vigorous stirring in a nitrogen atmosphere, followed by drip addition of concentrated ammonia solution (15 mL, 28%) to adjust the pH value to 9–10. After refluxing for one hour, we can get the carboxyl group functionalized ultrasmall Fe₃O₄ particles.

The resultant carboxyl unit on the surface of Fe₃O₄ nanoparticles was activated by N-(3-Dimethylaminopropyl)-N-ethylcarbodiimide (EDC) and N-Hydroxysuccinimide (NHS), and subsequently treated with AuNC-NH₂ to

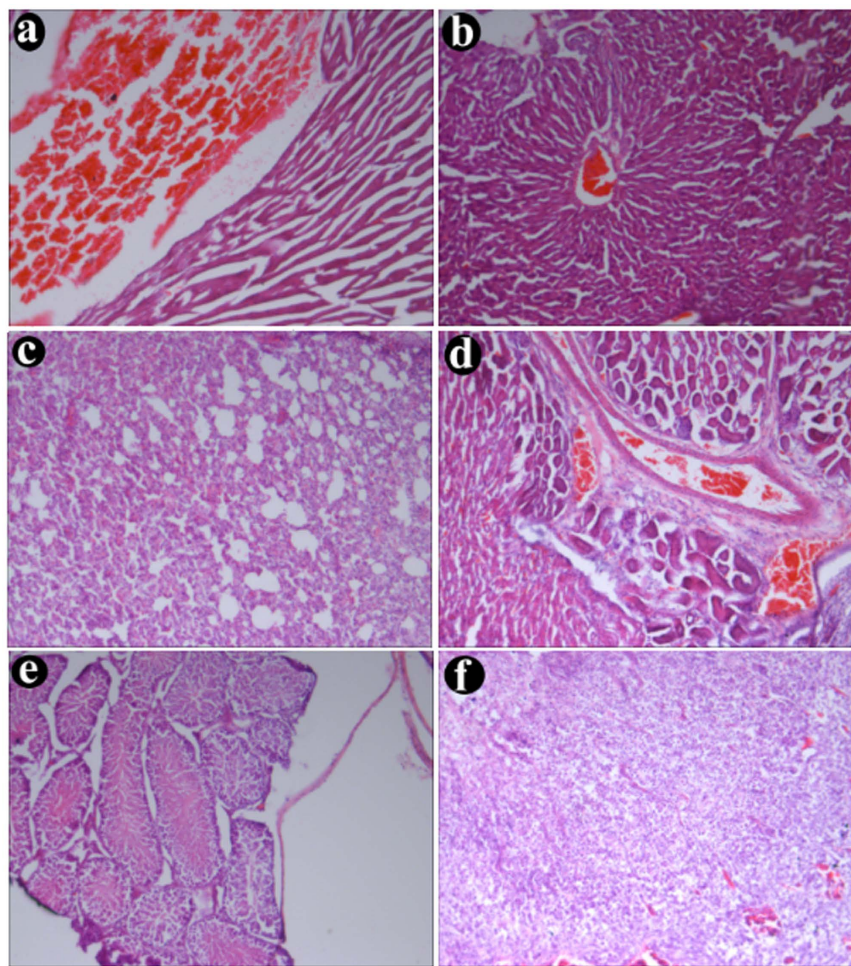


Figure 7. H&E staining of the organs sections (a) heart; (b) liver; (c) lung; (d) kidney; (e) bladder and (f) tumor) harvested from mice at 6 h post-injections.

obtain AuNC@Fe₃O₄. 10 mg of excessive ultrasamll Fe₃O₄ nanoparticles was reacted with 10 mg NHS and 20 mg EDC in 5 mL of water, stirring at room temperature for 30 min before adding to the 5 mg of AuNC-NH₂ suspension. Then the mixture was stirred at room temperature for another 24 h, followed by centrifugation and washing with ethanol and water, and then dispersed in 5 mL of ultra-purified water.

Bio-functionalized of AuNC@Fe₃O₄ with folic acid to form the F-AuNC@Fe₃O₄. AuNC@Fe₃O₄ were first functionalized with COOH-PEG-SH and then conjugated with biomolecular for *in vitro* and *in vivo* experiments. Briefly, 5.0 mL of prepared AuNC@Fe₃O₄ water solution was added to 5.0 mg of COOH-PEG-SH and reacted overnight at 4 °C under stirring. The excess COOH-PEG-SH was removed by centrifugation at 12000 rpm for 8 min and washed five times with water to obtain PEGylated AuNC@Fe₃O₄. The PEGylated AuNC@Fe₃O₄ was dispersed in 0.1 M (pH 7.4) phosphate buffer to remove any trace metal.

The bio-conjugation was performed by EDC-catalyzed peptide bond formation between the carboxyl group on the particle surface and amino group on folic acid. First, 10 mL of freshly prepared EDC solution (10 mg mL⁻¹ in weak acidic MES buffer solution) was mixed with 1 mL HNP solution with stirring for one hour. Then, 50 mL folic acid solution (containing 0.4% NaOH) was added to the solution and mixed well on a vortex, and then the above mixture was left on a rotary shaker overnight at room temperature. After that, the Triton-X 100 (0.25% (w/v), 20 mL) and BSA (2% (w/v), 20 mL) were added. The mixture was then left on the rotary shaker for one hour. Finally, the resulting folic acid functionalized AuNC@Fe₃O₄ (F-AuNC@Fe₃O₄) were separated from free biomolecules by gel filtration using Sephacryl HR-300 gel medium.

***In vitro* cytotoxicity study.** Human lung adenocarcinoma A549 cells and human umbilical vein endothelial cells (HUVEC) were cultured in 25 cm² flasks in Dulbecco's Modified Eagle's Medium DMEM (Gibco) containing 10% (v/v) fetal bovine serum (Gibco) at 37 °C in an atmosphere of 5% (v/v) CO₂ in air. The media were changed every two days, and the cells were passaged by trypsinization before confluence. Before experiment, the cells were pre-cultured until confluence was reached. For studying the cytotoxicity, both A549 and HUVEC cells were seeded in a 96-well plate at a density 10⁴ cells/well for 24 h at 37 °C in 5% CO₂. Then, the cells were treated with F-AuNC@Fe₃O₄ at different concentrations of 100, 200, 300, 400, 500 and even 1000 μg mL⁻¹. After incubation

for 24 h, cell viabilities were tested by standard MTT (3-(4,5)-dimethylthiazoliazol-2-yl)-2,5-diphenyltetrazolium bromide) assay. Cells incubated in the absence of nanoparticles were used as a control. All experiments were performed in triplicate.

Hemolysis assay. In order to detect whether F-AuNC@Fe₃O₄ will cause damage to red blood cells (RBCs) after being injected into the blood vessels, a hemolysis assay experiment was carried out. The red blood cells were obtained by removing serum from the blood by centrifugation and suction. The 0.5 mL cells suspension was then mixed with: (a) 1 mL of PBS as a negative control; (b) 1 mL deionized water as a positive control; (c) 1 mL nanoparticle PBS solution with different concentrations of 100, 200, 400, 800 and 1000 μg mL⁻¹. The mixtures were then vortexed for 2 h at room temperature. The samples were centrifuged and the absorbance spectrum of the supernatants was measured by UV-Vis characterization.

In vitro targeting cellular imaging. For to evaluate targeting capabilities of the F-AuNC@Fe₃O₄, the fluorescence Cy5-PEG-SH was used to track the F-AuNC@Fe₃O₄. Firstly, the mixture of COOH-PEG-SH and fluorescence Cy5-PEG-SH with 9:1 ratio was used to functionalize the surface of AuNC@Fe₃O₄, and then fluorescence AuNC@Fe₃O₄ was conjugation with targeting molecular folic acid to form the fluorescence F-AuNC@Fe₃O₄ for targeting cancer cell. All of the modified procedures can be done as described above. In the next step, the A549 cells (1 × 10⁵ cells per well) were cultured in confocal imaging chambers (NET) at 37 °C for 24 h, then 200 μL of F-AuNC@Fe₃O₄ and AuNC@Fe₃O₄ (without bio-conjugation) with a concentration of 0.5 mg mL⁻¹ were added to the chambers. After incubation for one hour, the cells were washed with a large amount of PBS to remove any free nanoparticles attached on the cell membrane and then stained with DAPI (10 μg mL⁻¹) for 20 min, rinsed with PBS at least three times. And then, the Olympus-FluoView FV10 confocal laser scanning microscope was used to image morphology of the A549 cells and track the F-AuNC@Fe₃O₄ location in the A549 cells.

In vivo CT, T₁ and T₂-weight MRI tri-modal imaging. Male BALB/c nude mice (4–6 weeks old) were purchased from the Cancer Institute & Hospital, Chinese Academy of Medical Sciences, Beijing. The Lung cancer A549 tumor-bearing models were generated by subcutaneous injection of 5 × 10⁶ cells in 50 μL of phosphate buffer solution (PBS) onto the left upper armpit of each mice. All the animal experiments were conducted in accordance with the guidelines of the Regional Ethics Committee, Liaoning Medical University, Liaoning Province, China. Firstly, the mice were anesthetized using 10% chloral hydrate (50 mL). Subsequently, 10 mg of F-AuNC@Fe₃O₄ dispersion solution was injected through the tail vein into the mouse. *In vivo* multi-imaging was performed at appropriate time points after tail vein injection.

CT imaging was acquired using Mediso nanoScan SPECT/CT produced by Mediso Ltd. Imaging parameters were as follows: slice thickness, medium; tube energy, 50 kVp, 670 μA; CT DIvol, 7279.9 cGy; semicircular parameters, full scan; Number of projections, 480; In-plane voxel size, medium. All animals were scanned in the cranial to caudal direction from the lower chest to the pelvis. CT data were analyzed using the Hounsfield units (HU) for regions.

In vivo MR imaging experiments were performed on a 3.0 T small animal MRI instrument (US Varian 3.0 T), and the pulse sequence used was a T₁-weighted SE-XL/90 sequence with the following parameters: TR = 482 ms, TE = 16 ms; field of view [FOV]: 40 × 90 cm; matrix: 256 × 256; number of excitations (NEX): 5; slice thickness = 1 mm; FOV: 40 × 90 cm; coil: VOLUME; T₂-weighted FSE-XL/90 sequence with the following parameters: TR = 3000 ms, TE = 48 ms; field of view [FOV]: 40 × 90 cm; matrix: 256 × 256; number of excitations (NEX): 5; slice thickness = 1 mm; FOV: 40 × 90 cm; coil: VOLUME.

Biodistribution of F-AuNC@Fe₃O₄. To assess the specific *in vivo* tumor targeting of F-AuNC@Fe₃O₄, After injected with 10 mg F-AuNC@Fe₃O₄, the tumor bearing mice were sacrificed at 6 h post-administration and the tissues including heart, kidney, liver, spleen and tumor were harvested for isolated organ imaging.

Histological study. Potential acute cytotoxicity and bio-distribution in major organs (heart, liver, lung, kidney, bladder and tumor) of tumor bearing mice post intravenous injection were assessed by dissection. Typical organs were harvested from the rats and immobilized in 4% paraformaldehyde at 4 °C for 48 h, and then embedded into paraffin. Sections from the organs were stained with hematoxylin and eosin (H&E) and observed under a light microscope at 100× magnification by an experienced physician, and representative images were provided.

References

- Chen, W., Zhuang, H., Cheng, G., Torigian, D. A. & Alavi, A. Comparison of FDG-PET, MRI and CT for post radiofrequency ablation evaluation of hepatic tumors. *Ann Nucl Med* **27**, 58–64 (2013).
- Zhang, Y. M., Jeon, M., Rich, L. J., Hong, H., Geng, J. M. *et al.* Non-invasive, multimodal functional imaging of the intestine with frozen micellar naphthalocyanines. *Nat Nanotechnol* **9**, 631–638 (2014).
- Weissleder, R. & Pittet, M. J. Imaging in the era of molecular oncology. *Nature* **452**, 580–589 (2008).
- Zhao, H. Y., Liu, S., He, J., Pan, C. C., Li, H. *et al.* Synthesis and application of strawberry-like Fe₃O₄-Au nanoparticles as CT-MR dual-modality contrast agents in accurate detection of the progressive liver disease. *Biomaterials* **51**, 194–207 (2015).
- Huang, J., Guo, M., Ke, H., Zong, C., Ren, B. *et al.* Rational design and synthesis of γ-Fe₂O₃@Au magnetic gold nanoflowers for efficient cancer theranostics. *Adv Mater* **27**, 5049–5056 (2015).
- Amendola, V., Scaramuzza, S., Litti, L., Meneghetti, M., Zuccolotto, G. *et al.* Magneto-plasmonic Au-Fe alloy nanoparticles designed for multimodal SERS-MRI-CT imaging. *Small* **10**, 2476–2486 (2014).
- Zhu, J., Lu, Y. J., Li, Y. G., Jiang, J., Cheng, L. *et al.* Synthesis of Au-Fe₃O₄ heterostructured nanoparticles for *in vivo* computed tomography and magnetic resonance dual model imaging. *Nanoscale* **6**, 199–202 (2014).
- Liu, G., Gao, J. H., Ai, H. & Chen, X. Y. Applications and potential toxicity of magnetic iron oxide nanoparticles. *Small* **9**, 1533–1545 (2013).
- Wang, G. N., Zhang, X. J., Skallberg, A., Liu, Y. X., Hu, Z. J. *et al.* One-step synthesis of water-dispersible ultra-small Fe₃O₄ nanoparticles as contrast agents for T₁ and T₂ magnetic resonance imaging. *Nanoscale* **6**, 2953–2963 (2014).

10. He, X. X., Liu, F. Y., Liu, L., Duan, T. C., Zhang, H. M. *et al.* Lectin-conjugated Fe₂O₃@Au core@shell nanoparticles as dual mode contrast agents for *in vivo* detection of tumor. *Mol. Pharm.* **11**, 738–745 (2014).
11. Li, J. C., Hu, Y., Yang, J., Wei, P., Sun, W. J. *et al.* Hyaluronic acid-modified Fe₃O₄@Au core/shell nanostars for multimodal imaging and photothermal therapy of tumors. *Biomaterials* **38**, 10–21 (2015).
12. Skrabalak, S. E., Au, L., Li, X. D. & Xia, Y. N. Facile synthesis of Ag nanocubes and Au nanocages. *Nature Protocols* **2**, 2182–2190 (2007).
13. Bao, F., Yao, J. L. & Gu, R. A. Synthesis of magnetic Fe₂O₃/Au core/shell nanoparticles for bioseparation and immunoassay based on surface-enhanced raman spectroscopy. *Langmuir* **25**, 10782–10787 (2009).
14. Shi, P., Li, M., Ren, J. S. & Qu, X. G. Gold Nanocage-based dual responsive “caged metal chelator” release system: noninvasive remote control with near infrared for potential treatment of alzheimer’s disease. *Advanced Functional Materials* **43**, 5412–5419 (2013).
15. Xie, J. P., Zhang, Q. B., Lee, J. Y. & Wang, D. I. C. The synthesis of SERS-active gold nanoflower tags for *in vivo* applications. *ACS Nano* **2**, 2473–2480 (2008).
16. Cole, L. E., Ross, R. D., Tilley, J. M., Vargo-Gogola, T. & Roeder, R. K. Gold nanoparticles as contrast agents in x-ray imaging and computed tomography. *Nanomedicine* **10**, 321–341 (2015).
17. Sathe, T. R., Agrawal, A. & Nie, S. M. Mesoporous silica beads embedded with semiconductor quantum dots and iron oxide nanocrystals: dual-function microcarriers for optical encoding and magnetic separation. *Anal Chem* **78**, 5627–5632 (2006).
18. Xiao, Q., Bu, W., Ren, Q., Zhang, S., Xing, H. *et al.* Radiopaque fluorescence-transparent TaO_x decorated upconversion nanophosphors for *in vivo* CT/MR/UCL trimodal imaging. *Biomaterials* **33**, 7530–7539 (2012).
19. Feng, Y., Zong, Y. D., Ke, T. Y., Jeong, E. K., Parker, D. L. *et al.* Pharmacokinetics, biodistribution and contrast enhanced MR blood pool imaging of Gd-DTPA cystine copolymers and Gd-DTPA cystine diethyl ester copolymers in a rat mode. *Model. Pharm. Res.* **23**, 1736–1742 (2006).
20. Tombach, B., Reimer, P., Bremer, C., Allkemper, T., Engelhardt, M. *et al.* First-pass and equilibrium-MRA of the aortoiliac region with a superparamagnetic iron oxide blood pool MR contrast agent (SHU 555C): results of a human pilot study. *NMR Biomed.* **17**, 500–506 (2004).
21. Bjørnerud, A. & Johansson, L. The utility of superparamagnetic contrast agents in MRI: theoretical consideration and applications in the cardiovascular system. *NMR Biomed.* **17**, 465–477 (2004).
22. Linderoth, S., Hendriksen, P. V., Bødker, F., Wells, S., Davies, K. *et al.* On spin-canting in maghemite particles. *J Appl. Phys.* **75**, 6583–6585 (1994).

Acknowledgements

We gratefully acknowledge support from National Natural Science Foundation of China (No. 81401499) and Start-up grant of University of Macau (SRG2015-00007-FHS).

Author Contributions

G.N.W. and X.M. conceived the idea and designed the experiments. G.N.W. and G.W. fabricated the samples and carried out *in vitro* and *in vivo* experiments. X.Z. and X.M. performed new contrast agent measurements and analyzed the results. G.N.W., X.Z. and X.M. discussed the results and wrote the manuscript.

Additional Information

Supplementary information accompanies this paper at <http://www.nature.com/srep>

Competing financial interests: The authors declare no competing financial interests.

How to cite this article: Wang, G. *et al.* Au Nanocage Functionalized with Ultra-small Fe₃O₄ Nanoparticles for Targeting T₁-T₂ Dual MRI and CT Imaging of Tumor. *Sci. Rep.* **6**, 28258; doi: 10.1038/srep28258 (2016).



This work is licensed under a Creative Commons Attribution 4.0 International License. The images or other third party material in this article are included in the article’s Creative Commons license, unless indicated otherwise in the credit line; if the material is not included under the Creative Commons license, users will need to obtain permission from the license holder to reproduce the material. To view a copy of this license, visit <http://creativecommons.org/licenses/by/4.0/>